



Heme Oxygenase-1-Modified BMMSCs Activate AMPK–Nrf2–FTH1 to Reduce Severe Steatotic Liver Ischemia–Reperfusion Injury

Xiaorong Tian¹ · Yuxin Wang¹ · Mengshu Yuan¹ · Weiping Zheng^{2,3} · Huaiwen Zuo¹ · Xinru Zhang¹ · Hongli Song^{2,4}

Received: 15 April 2023 / Accepted: 28 August 2023 / Published online: 14 September 2023
© The Author(s) 2023

Abstract

Background Ischemia–reperfusion injury (IRI) is an important cause of graft dysfunction post-liver transplantation, where donor liver with severe steatosis is more sensitive to IRI. Liver IRI involves ferroptosis and can be alleviated by heme oxygenase-1-modified bone marrow mesenchymal stem cells (HO-1/BMMSCs).

Aims To explore the role and mechanism of HO-1/BMMSCs in severe steatotic liver IRI.

Methods A severe steatotic liver IRI rat model and a hypoxia/reoxygenation (H/R) of severe steatosis hepatocyte model were established. Liver and hepatocyte damage was evaluated via liver histopathology and cell activity. Ferroptosis was evaluated through ferroptosis indexes. Nuclear factor erythroid 2-related factor 2 (Nrf2) was knocked down in severe steatotic hepatocytes. The role of Nrf2 and AMPK in HO-1/BMMSC inhibition of ferroptosis was examined using the AMP-activated protein kinase (AMPK) pathway inhibitor Compound C.

Results The HO-1/BMMSCs alleviated severe steatotic liver IRI and ferroptosis. HO-1/BMMSCs promoted ferritin heavy chain 1 (FTH1), Nrf2, and phosphorylated (p)-AMPK expression in the H/R severe steatotic hepatocytes. Nrf2 knockdown decreased FTH1 expression levels but did not significantly affect p-AMPK expression levels. The protective effect of HO-1/BMMSCs against H/R injury in severe steatotic hepatocytes and the inhibitory effect on ferroptosis were reduced. Compound C decreased p-AMPK, Nrf2, and FTH1 expression levels, weakened the HO-1/BMMSC protective effect against severe steatotic liver IRI and H/R-injured severe steatotic hepatocytes, and reduced the inhibition of ferroptosis.

Conclusions Ferroptosis was involved in HO-1/BMMSC reduction of severe steatotic liver IRI. HO-1/BMMSCs protected against severe steatotic liver IRI by inhibiting ferroptosis through the AMPK–Nrf2–FTH1 pathway.

Graphical Abstract

HO-1/BMMSCs activate AMPK, which activates Nrf2, promotes its nuclear transcription, then promotes the expression of its downstream protein FTH1, thereby inhibiting ferroptosis and attenuating severe steatotic liver IRI in rats. Glu: glutamic acid; Cys: cystine; GSH: glutathione; GPX4: glutathione peroxidase 4; HO-1/BMMSCs: HO-1-modified BMMSCs; Fer-1:

✉ Hongli Song
hlsong26@163.com; songhl@tmu.edu.cn

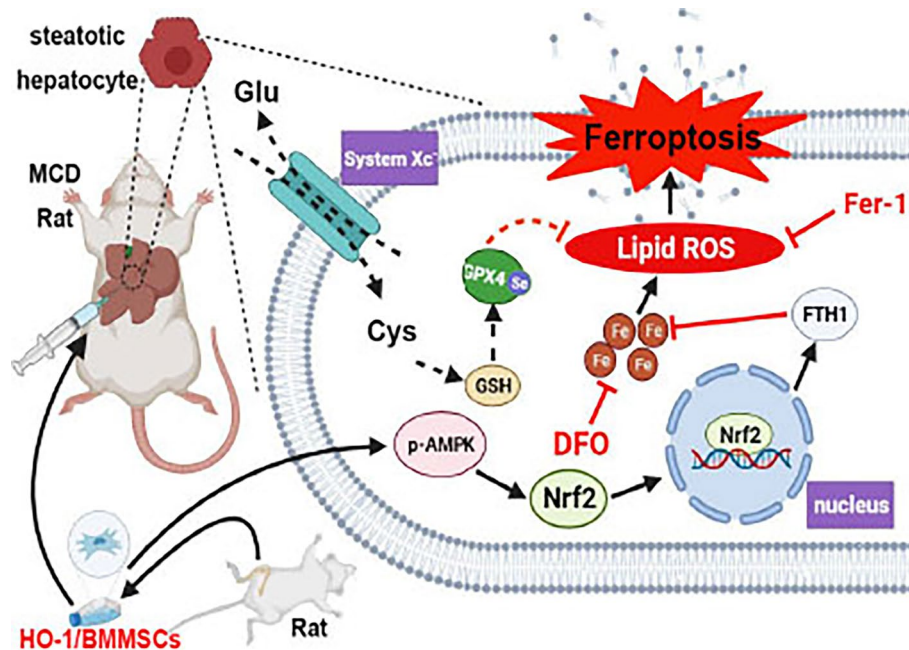
¹ Tianjin First Central Hospital Clinic Institute,
Tianjin Medical University, Tianjin 300070,
People's Republic of China

² Department of Organ Transplantation, Tianjin First
Central Hospital, School of Medicine, Nankai University,
Tianjin 300192, People's Republic of China

³ NHC Key Laboratory of Critical Care Medicine,
Tianjin 300192, People's Republic of China

⁴ Tianjin Key Laboratory of Organ Transplantation,
No. 24 Fukang Road, Nankai District, Tianjin 300192,
People's Republic of China

ferrostatin-1; DFO: deferoxamine; FTH1: ferritin heavy chain1; p-AMPK: phosphorylated AMP-activated protein kinase; Nrf2: nuclear factor erythroid 2-related factor 2; IRI: ischemia-reperfusion injury; MCD: methionine-choline deficiency



Keywords Ferroptosis · Bone marrow mesenchymal stem cells · Ischemia–reperfusion injury · Liver steatosis · AMPK–Nrf2–FTH1

Introduction

The shortage of donor liver remains a significant challenge for liver transplantation [1]. The increasing incidence of liver steatosis in the population [2] affects donor liver quality, and severe steatotic liver transformation increases the possibility of steatotic liver and kidney failure in recipients [3]. Ischemia–reperfusion (I/R) injury (IRI) is an important cause of graft dysfunction after liver transplantation [4], where severe steatotic liver is more sensitive to IRI [5, 6]. Therefore, it is of great importance to explore the methods and mechanisms of alleviating IRI in severe steatotic liver transplantation to enable its successful application in the clinic.

Bone marrow mesenchymal stem cells (BMMSCs) have the functions of immune regulation, anti-inflammatory and repair of damaged organs [7, 8]. Heme oxygenase-1 (HO-1) is a cytoprotective enzyme whose modification of BMMSCs (HO-1/BMMSCs) enhanced BMMSC viability, prolonged BMMSC survival time at the damaged site, and protected the graft [7].

In recent years, ferroptosis was observed in IRI in various organs [9–11]. Ferroptosis is an iron-dependent form

of cell death caused by the accumulation of lipid reactive oxygen species (ROS) that differs from apoptosis, pyroptosis, and necrosis [12]. Ferroptosis is inhibited by a ferroptosis inhibitor, ferrostatin-1 (Fer-1), and an iron chelating agent, deferoxamine (DFO). Glutathione peroxidase 4 (GPX4) maintains intracellular redox homeostasis, which can convert toxic lipid hydroperoxides into non-toxic lipid alcohols, thereby inhibiting ferroptosis [13, 14]. IRI is related to oxidative stress, and oxidative damage is also a main cause of ferroptosis [15]. Furthermore, steatotic liver IRI also features oxidative stress and abnormal expression of iron-related protein metabolism [16]. Therefore, regulating ferroptosis may be an effective method to alleviate IRI damage in steatotic liver.

Nuclear factor erythroid 2-related factor 2 (Nrf2) is the main regulator of redox homeostasis in many liver diseases [17] that is activated by AMP-activated protein kinase (AMPK), which drives its antioxidant effect [18]. Therefore, we explored the protective effect of HO-1/BMMSCs on severe steatotic liver IRI in rats and its possible mechanism to suggest a new treatment method for alleviating severe steatotic liver IRI and provide a research direction to expand the donor liver pool.

Materials and Methods

Animals

Specific pathogen-free (SPF) male Sprague–Dawley (SD) rats (4–5 weeks old, 40–70 g) were purchased from the China Food and Drug Administration (Beijing, China) for BMMSC preparation. The severe steatotic liver models were established using 36 rats (7–8 weeks old, 240–260 g). All rats were housed in an environment containing appropriate humidity and temperature in a 12-h light–dark cycle and with free access to feed and water.

Extraction of BMMSCs and Identification of HO-1/BMMSCs

BMMSCs were aseptically extracted from the SD rat bilateral femurs and tibias. The BMMSCs were selected through adherent culture and cultured to the third generation. Adenovirus carrying the *HO1* gene/green fluorescent protein (GFP) (GeneChem, Shanghai, China) was transfected into the third-generation BMMSCs at a 1:10 ratio. The HO-1/BMMSCs morphology was observed under a light microscope. The HO-1/BMMSC biological characteristics were determined by inducing lipogenesis and osteogenesis in vitro. The HO-1/

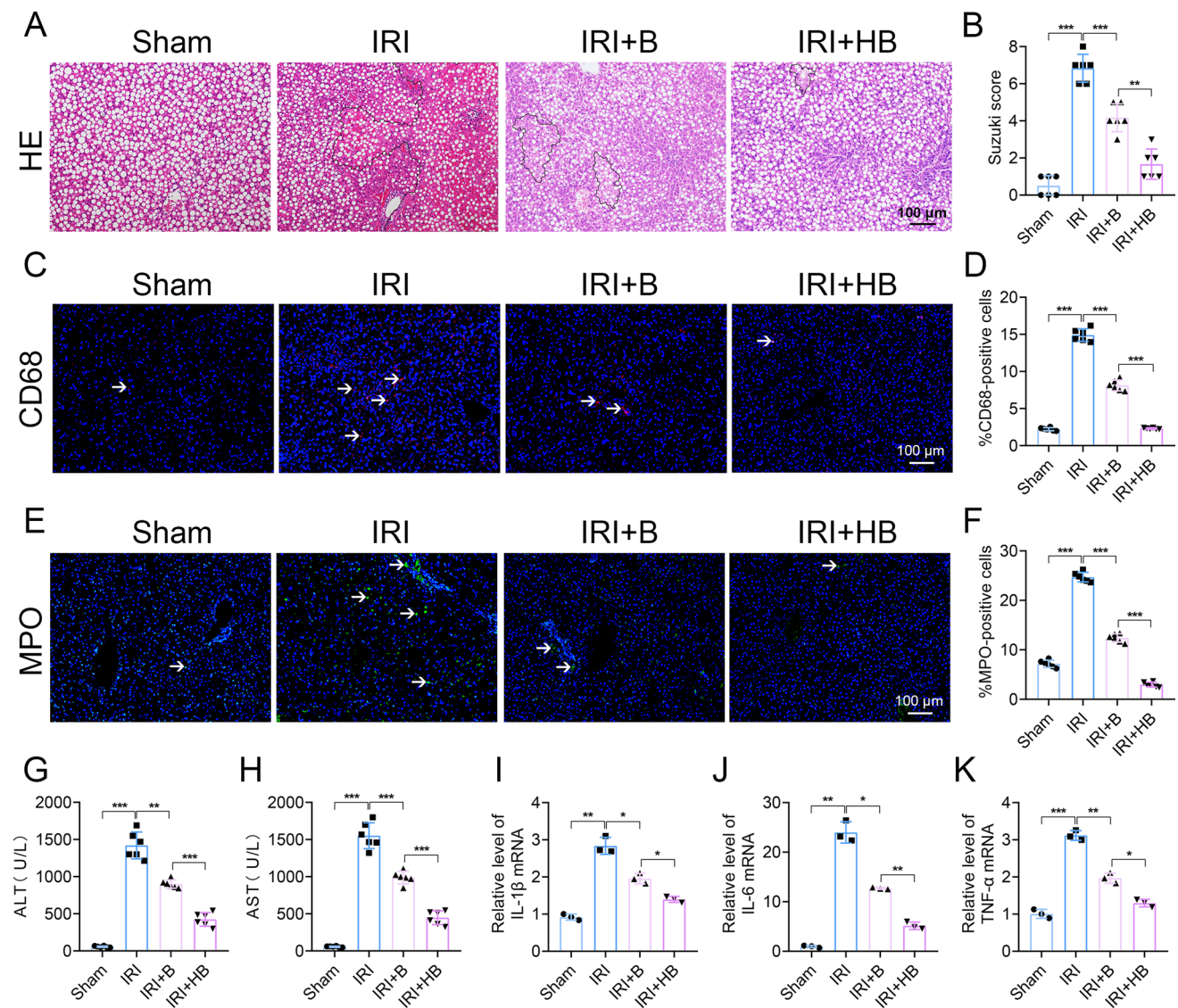


Fig. 1 Protective effect of HO-1/BMMSCs on severe steatotic liver IRI. **A** Liver histopathology ($\times 100$). **B** Suzuki score of liver tissue. **C** CD68 expression (red) in liver tissue ($\times 100$). White arrows indicate positive-expression cells. **D** CD68 expression in liver tissue. **E** MPO expression (green) in liver tissue ($\times 100$). White arrows indicate posi-

tive-expression cells. **F** MPO expression in liver tissue. **G, H** Expression of ALT (**G**) and AST (**H**) liver enzymes in serum. **I, J, K** IL-1 β (**I**), IL-6 (**J**), and TNF- α (**K**) expression levels in liver tissue. $n = 6$ per group. * $p < 0.05$, ** $p < 0.01$, *** $p < 0.001$

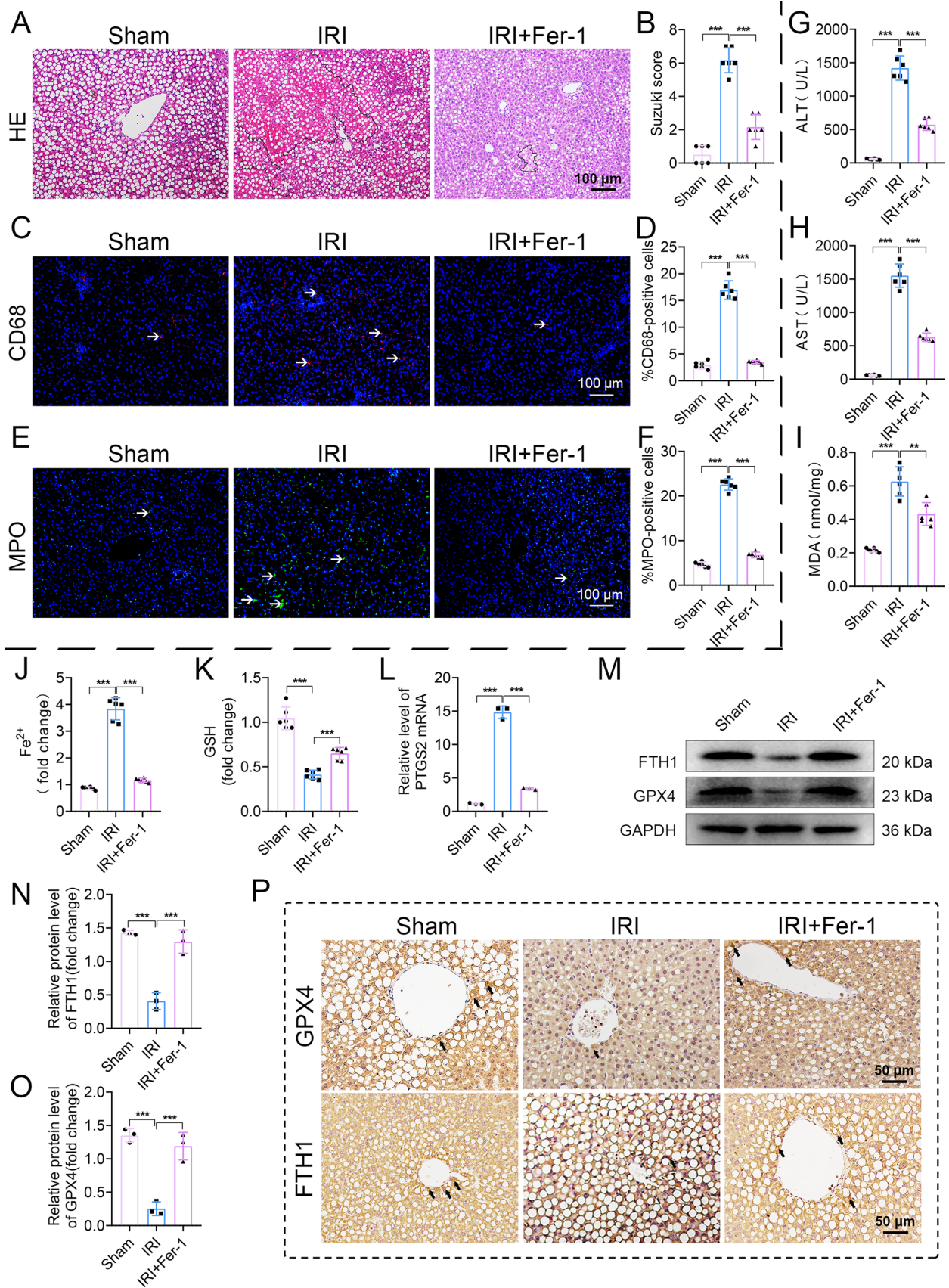


Fig. 2 Relationship between ferroptosis and severe steatotic liver IRI in rats. **A** Liver histopathology ($\times 100$). **B** Suzuki score of liver tissue. **C** CD68 expression (red) in liver tissue ($\times 100$). White arrows indicate positive-expression cells. **D** CD68 expression level in liver tissue. **E** MPO expression (green) in liver tissue ($\times 100$). White arrows indicate positive-expression cells. **F** MPO expression level in liver tissue. **G, H** Expression levels of ALT (**G**) and AST (**H**) liver enzymes in serum. **I** MDA expression level in liver tissue. **J** Fe^{2+} expression level in liver tissue. **K** GSH expression level in liver tissue. **L** PTGS2 expression level in liver tissue. **M, N, O** FTH1 (**N**) and GPX4 (**O**) protein expression levels in liver tissue. **P** Detection of FTH1 and GPX4 protein in liver tissue ($\times 200$). Black arrows indicate positive-expression cells. $n=6$ per group. $*p < 0.05$, $**p < 0.01$, $***p < 0.001$

BMMSC cell phenotype was identified by flow cytometry using the anti-cluster differentiation antibodies (CD) 29, CD90, CD34, CD45, RT1A, and RT1B (BioLegend, San Diego, CA, USA). HO-1/BMMSCs emitting green fluorescence were observed under a fluorescence microscope to determine the adenovirus transfection efficiency. The *HO1* gene expression was verified by qRT-PCR and western blotting [19] (see Table S1 and Table S2 for HO-1 gene and protein information).

Construction of Rat Model of Severe Steatotic Liver IRI

The SD rats were fed with methionine-choline deficiency (MCD) feed, during which the animals drank and ate freely. After 14 days, the rat model of severe steatotic liver was established and identified by hematoxylin–eosin (HE) and oil red O staining. Rats with severe steatotic liver disease were fasted 12 h before surgery and drank freely. After anesthesia, the left and middle lobe hepatic arteries and portal vein branches of the hilar region were blocked with noninvasive arterial clamps, resulting in an ischemic range of 70%. After 80-min warm ischemia, the arterial clamp was opened and the animals were reperfused for 24 h [20]. The animals were randomly divided into six groups ($n=6$ rats per group): sham operation (Sham), IRI, IRI + Fer-1, IRI + BMMSCs (IRI + B), IRI + HO-1/BMMSCs (IRI + HB), and IRI + HB + Compound C (IRI + HB + C–C). The Sham group underwent only open and closed abdominal operations; the IRI + Fer-1 rats were intraperitoneally injected with 5 mg/kg Fer-1 (MCE, Shanghai, China) 1 day before surgery and during reperfusion; the IRI + B and IRI + HB rats were injected through the caudal vein and portal vein 1 day before surgery and during reperfusion, respectively, with 2×10^6 BMMSCs or HO-1/BMMSCs; the IRI + HB + C–C rats received intraperitoneal injection of 2 mg/kg Compound C (MCE) 1 h before surgery. The

remaining treatments were the same as those of the IRI + HB group.

In Vivo Tracing of HO-1/BMMSCs

The BMMSCs were transfected with adenoviruses carrying GFP or HO-1/GFP. During severe steatotic liver reperfusion, the transfected cells were injected into the rats through the portal vein. After 24-h reperfusion, frozen sections were obtained from the liver tissues of the GFP/BMMSC- or GFP/HO-1/BMMSC-treated severe steatotic liver rats treated. Under a fluorescence microscope, the cells that emitted green fluorescence were used for colonization.

Establishment of a Hepatocyte Model of Steatosis

Rat hepatocytes (IAR20) were inoculated into a 6-well plate and cultured in Minimal Essential Medium (MEM) (Gibco, Thermo Fisher Scientific, Waltham, MA, USA) containing 10% fetal bovine serum (FBS, Biotest Inc., Nuaille, France) and 1% penicillin. When the fusion rate was 50–60%, 200 μM sodium oleate (Sigma-Aldrich, St. Louis, MO, USA) and 100 μM sodium palmitate (Aladdin Biochemical Technology Co. Ltd., Shanghai, China) were added and the cells were incubated in a cell incubator containing 5% CO_2 for 12, 24, and 36 h. After staining, the cells were observed and photographed under a microscope in accordance with the operating instructions for oil red O staining solution (Solarbio, Beijing, China).

Construction of Steatotic Hepatocyte Hypoxia/Reoxygenation (H/R) Model

The adipocyte culture medium was replaced with blank medium without serum. After 24-h starvation, the cells were placed in an anoxic chamber containing 94% N_2 , 5% CO_2 , and 1% O_2 (MIC-101; Billups-Rothenberg, San Diego, CA, USA) and cultured for 2, 6, 12, and 24 h, respectively. Then, the blank medium was replaced with complete culture medium, and the cells were cultured for 6 h in a cell incubator containing 5% CO_2 . The cell activity measurement results indicated that the H/R time node was 6 h/6 h.

Co-culture

The hepatocytes were inoculated into a 6-well plate (3×10^5 cells/well), then a 0.4- μm Transwell chamber (Corning, GE Inc., Hartford, CT, USA) was placed on the 6-well plate. BMMSCs or HO-1/BMMSCs (1×10^6 cells/well) were inoculated in the upper layer of the Transwell chamber and cultured 24 h.

Small Interfering RNA (siRNA) Transfection

The siRNAs were synthesized by Ji Ma Gene Co., Ltd. (Shanghai, China) and Table S3 lists the specific sequence. Steatotic hepatocytes were inoculated on a 6-well plate, grown to 70% confluence, and transfected with siRNA according to the instructions of siRNA-Mate transfection reagent (Ji Ma Gene Co., Ltd.). The siRNA optimal concentration for gene silencing was 100 nM. The transfection efficiency was detected by qRT-PCR and western blotting.

Liver Function

The serum of the rats in each treatment group was collected and the alanine aminotransferase (ALT), aspartate aminotransferase (AST), total bilirubin (TBIL), and lactate dehydrogenase (LDH) levels were measured using a fully automated biochemical analyzer (Cobas 800; Roche Diagnostics, Basel, Switzerland).

HE Staining

The rat liver tissue was immersed in 10% formalin, embedded in wax, sectioned consecutively, and stained with HE. The liver tissue damage was observed under a light microscope. Five microscope fields ($\times 100$ magnification) were randomly selected for observation and scored based on the Suzuki score [21]. Table S4 depicts the Suzuki scoring table.

Immunohistochemistry and Immunofluorescence Staining

The liver tissues were stained with immunohistochemistry and immunofluorescence according to a previously described method [16, 22]. Immunohistochemistry was used to detect the expression of GPX4 (1:2000, Proteintech, Wuhan, China) and ferritin heavy chain 1 (FTH1, 1:300, Bioss, Beijing, China), while immunofluorescence was used to detect the expression of CD68 (1:100, Santa Cruz Biotechnology, Dallas, TX, USA) and myeloperoxidase (MPO, 1:100, Proteintech).

Cell immunofluorescence staining was performed according to our previously described method [22] to detect the expression of FTH1 (1:100, Bioss), Nrf2 (1:200, Cell Signaling Technology, Boston, MA USA), and phosphorylated (p)-AMPK (1:100, Bioss).

Detection of Fe²⁺, Malondialdehyde (MDA), and Glutathione (GSH)

The Fe²⁺, MDA, and GSH contents were detected with an iron assay kit (Abcam, Cambridge, UK), MDA detection kit (Beyotime, Shanghai, China), and GSH detection kit

(Solarbio, Beijing, China), respectively. The absorbance was measured at 593 nm, 532 nm, and 412 nm for statistical analysis.

Western Blotting

The total protein of the liver tissue and hepatocytes was extracted with radioimmunoprecipitation assay buffer. The protein concentration was determined with the bicinchoninic acid method, and western blotting was performed as previously described [22]. The primary antibodies were those against HO-1 (1:1000, Proteintech), GPX4 (1:5000, Proteintech), FTH1 (1:1000, Bioss), Nrf2 (1:1000, Cell Signaling Technology), p-AMPK (1:1000, Bioss), AMPK (1:1000, Proteintech), and GAPDH (1:15,000, Cell Signaling Technology). Protein expression was analyzed using ImageJ 7.0 (NIH, Bethesda, MD, USA).

RNA Extraction and qRT-PCR

Total RNA from liver tissue and hepatocytes was extracted using RNAiso Plus reagent (Takara, Shiga, Japan) according to the instructions of a reverse transcription and amplification kit (Takara). PTGS2, IL-1 β , IL-6, TNF- α , Nrf2, and HO-1 expression levels were detected. The internal reference was β -actin. All primers were synthesized by Sangon Biotech (Shanghai, China). Table S5 lists the primer sequences.

Cell Viability Assay

Cell viability was determined using Cell Counting Kit-8 (CCK8) according to the manufacturer's instructions (Solarbio). Briefly, 5×10^3 /well steatotic hepatocytes were seeded in 96-well plates and subjected to H/R, H/R + Fer-1, H/R + DFO, H/R + B, or H/R + HB. After H/R + HB + C–C treatment, the CCK8 reagent was added to detect the absorbance at 450 nm, then the cell viability of each treatment group was evaluated.

Lipid ROS and ROS Detection

Lipid ROS was measured using BODIPY-C11 dye (Invitrogen, Waltham, MA, USA). Hepatocytes (3×10^5 /well) were seeded in 12-well plates, steatosis was induced, then H/R, H/R + Fer-1, H/R + DFO, H/R + B, H/R + HB, or H/R + HB + C–C treatment was administered. Subsequently, the cells were incubated with BODIPY-C11 dye (5 μ M) at 37 °C in the dark for 20 min, digested for 1 min and washed three times, and the fluorescence intensity was measured by flow cytometry.

For the ROS measurement, 3×10^5 /well hepatocytes were inoculated in 12-well plates, treated as described earlier, then digested, washed, centrifuged, and resuspended. Then,

the cells were incubated with 10 μM dichlorodihydrofluorescein diacetate (DCFH-DA, Beyond Company, Shanghai, China) at 37 $^{\circ}\text{C}$ in the dark for 20 min. During this period, the plates were shaken well 2–3 times, centrifuged at 350 \times g for 5 min at 4 $^{\circ}\text{C}$, and washed. Fluorescence was detected on a flow cytometer (Accuri C6 Plus, Becton Dickinson, Franklin Lakes, NJ, USA).

Statistical Analysis

The data were analyzed using GraphPad Prism 8.0 (GraphPad Software, La Jolla, CA, USA). The experimental data conformed to the normal distribution, and all data are expressed as the mean \pm standard deviation. Two groups and multiple groups were compared with the independent sample *t* test and one-way analysis of variance (ANOVA), respectively. $P < 0.05$ was considered to indicate a statistically

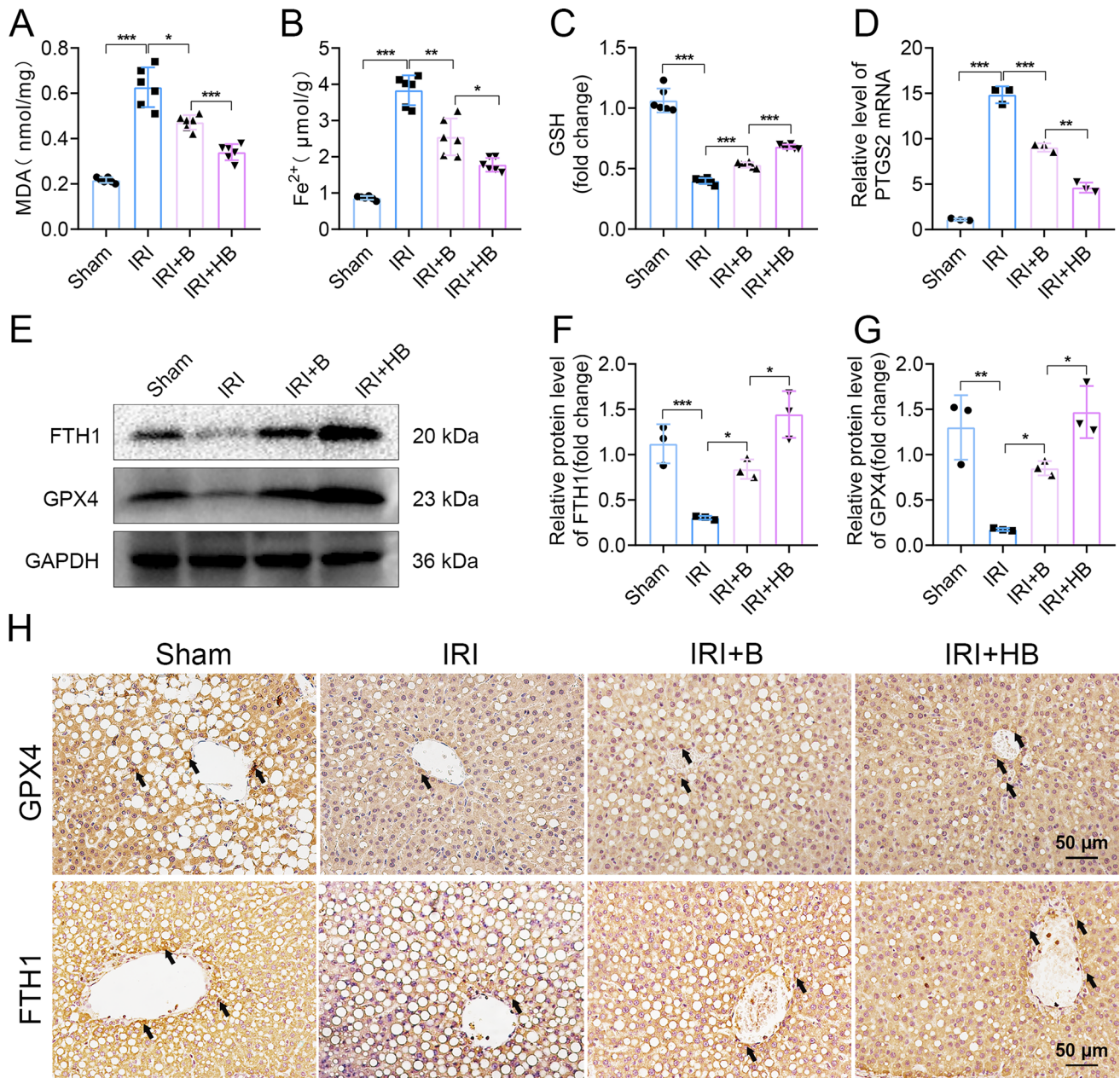


Fig. 3 Inhibitory effect of HO-1/BMMSCs on ferroptosis in steatotic liver of IRI rats. **A** MDA expression level in liver tissue. **B** Fe^{2+} expression level in liver tissue. **C** GSH expression level in liver tissue. **D** PTGS2 expression level in liver tissue. **E**, **F**, **G** FTH1 (**F**) and

GPX4 (**G**) protein expression levels in liver tissue. **H** Detection of FTH1 and GPX4 proteins in liver tissue ($\times 200$). Black arrows indicate positive-expression cells. $n = 6$ per group. * $p < 0.05$, ** $p < 0.01$, *** $p < 0.001$

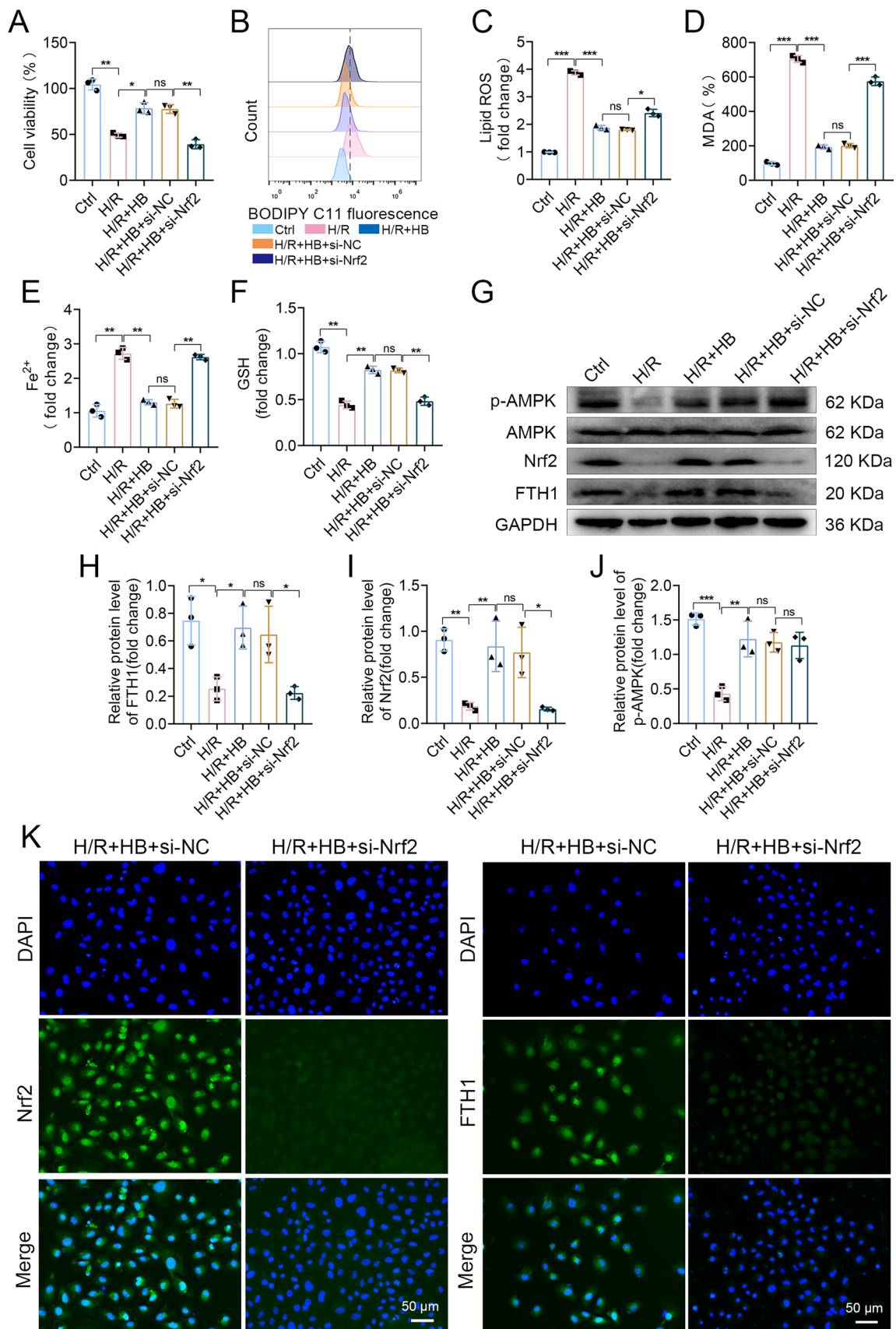


Fig. 4 HO-1/BMMSCs promote Nrf2 expression and inhibit ferroptosis. **A** Determination of steatotic hepatocyte activity. **B, C** Lipid ROS expression level in steatotic hepatocytes. **D** Relative MDA expression level in steatotic hepatocytes. **E** Relative Fe²⁺ expression level in steatotic hepatocytes. **F** Relative GSH expression level in steatotic hepatocytes. **G, H, I, J** FTH1 (**H**), Nrf2 (**I**), and p-AMPK (**J**) protein expression levels. **K** Nrf2 and FTH1 immunofluorescence results ($\times 200$). $n=3$ per group. ns, No statistical difference, $*p<0.05$, $**p<0.01$, $***p<0.001$

significant difference. Each experiment was repeated at least three times.

Results

Identification and Tracing of HO-1/BMMSCs and Establishment of Severe Steatotic Liver and IRI Rat Models

The typical spindle morphology of HO-1/BMMSCs was observed under light microscopy (Fig. S1A), where the HO-1/BMMSCs had lipid and osteogenic differentiation potential (Fig. S1B, S1C). CD90, CD29, and RT1A surface marker staining was positive in > 99% of the HO-1/BMMSCs, while more than 99% of the HO-1/BMMSCs were negative for the surface markers CD45, CD34, and RT1B (Fig. S1D–I). More than 85% of the HO-1/BMMSCs emitted green fluorescence (Fig. S1J). The HO-1/BMMSCs had significantly higher HO-1 expression than the BMMSCs (Fig. S1K–M).

Severe Steatotic Liver IRI Rat Model and Tracing of GFP/HO-1/BMMSCs In Vivo

Compared to the normal rat liver, the liver of rats with simple steatosis generally had greasy surfaces with blunt edges. After ischemia, the liver turned pale yellow and the liver surface appeared mottled after reperfusion (Fig. S2A). The steatotic liver sections demonstrated significant lipid droplets in the cytoplasm and > 60% fatty change (Fig. S2B). The normal liver had neatly arranged hepatocytes, normal liver lobule structure, no blood stasis in the liver sinuses, and no necrotic lesions in the tissue. The steatotic liver was observed as bullous fatty change without obvious necrotic lesions. The IRI group demonstrated obvious necrotic foci and severe hepatic sinus congestion (Fig. S2C). This indicated the successful construction of an SD rat steatotic liver ischemia reperfusion model. After 24-h reperfusion of GFP/BMMSCs and GFP/HO-1/BMMSCs, the BMMSCs and HO-1/BMMSCs were implanted in the liver, but HO-1/BMMSCs were more numerous than BMMSCs (Fig. S2D).

HO-1/BMMSCs Alleviated Severe Steatotic Liver IRI

Compared with the Sham group, the pathological sections of the severe steatotic liver in the IRI group exhibited obvious necrosis and more serious hepatic sinusoidal congestion. The BMMSC and HO-1/BMMSC intervention was followed by significantly improved liver tissue necrosis and hepatic sinusoidal congestion, where the HO-1/BMMSCs exerted a significantly better effect than the BMMSCs (Fig. 1A). Simultaneously, the BMMSCs and HO-1/BMMSCs improved the Suzuki score of the severe steatotic liver IRI, where the HO-1/BMMSCs exerted more significant improvement (Fig. 1B).

I/R significantly increased CD68 (macrophage surface marker) (Fig. 1C, D) and MPO (neutrophil surface marker) (Fig. 1E, F) expression in the severe steatotic liver. However, the BMMSCs and HO-1/BMMSCs reduced the CD68 and MPO expression. Further comparison demonstrated that the HO-1/BMMSCs exerted a more significant effect (Fig. 1C–F).

The BMMSCs and HO-1/BMMSCs also reduced the ALT, AST, TBIL, LDH, IL-1 β , IL-6 and TNF- α associated with IRI. The comparison demonstrated that HO-1/BMMSCs had stronger ability to reduce the levels of liver enzymes and inflammatory indicators (Fig. 1G–K, Fig. S3). These results demonstrated that the BMMSCs and HO-1/BMMSCs improved the severe steatotic liver IRI in rats and that HO-1/BMMSCs exerted a better improvement effect.

We successfully constructed a steatotic hepatocyte model (Fig. S4). Using the H/R model of severe steatotic hepatocytes in vitro to simulate the IRI process of severe steatotic liver in vivo, H/R (6 h/6 h) was selected for the experiment. The steatotic hepatocyte morphology and activity in the HO-1/BMMSC treatment group exhibited more significant improvement. The results suggested that HO-1/BMMSCs reduced the H/R damage of steatotic hepatocytes and that their repair effect was more significant than that of BMMSCs (Fig. S5).

Ferroptosis Was Involved in Severe Steatotic Liver IRI

The pathological liver sections from the Sham group exhibited normal histological structure. The IRI group had narrowed and congested hepatic sinuses, liver lobules that had lost their normal structure, and lamellar necrosis of the liver tissue. The Fer-1 treatment group had significantly reduced liver congestion, close to normal liver lobule structure, and significantly reduced tissue necrosis (Fig. 2A). The Suzuki score of the IRI group was significantly higher than that of the Sham group, while Fer-1 treatment significantly decreased the Suzuki score (Fig. 2B).

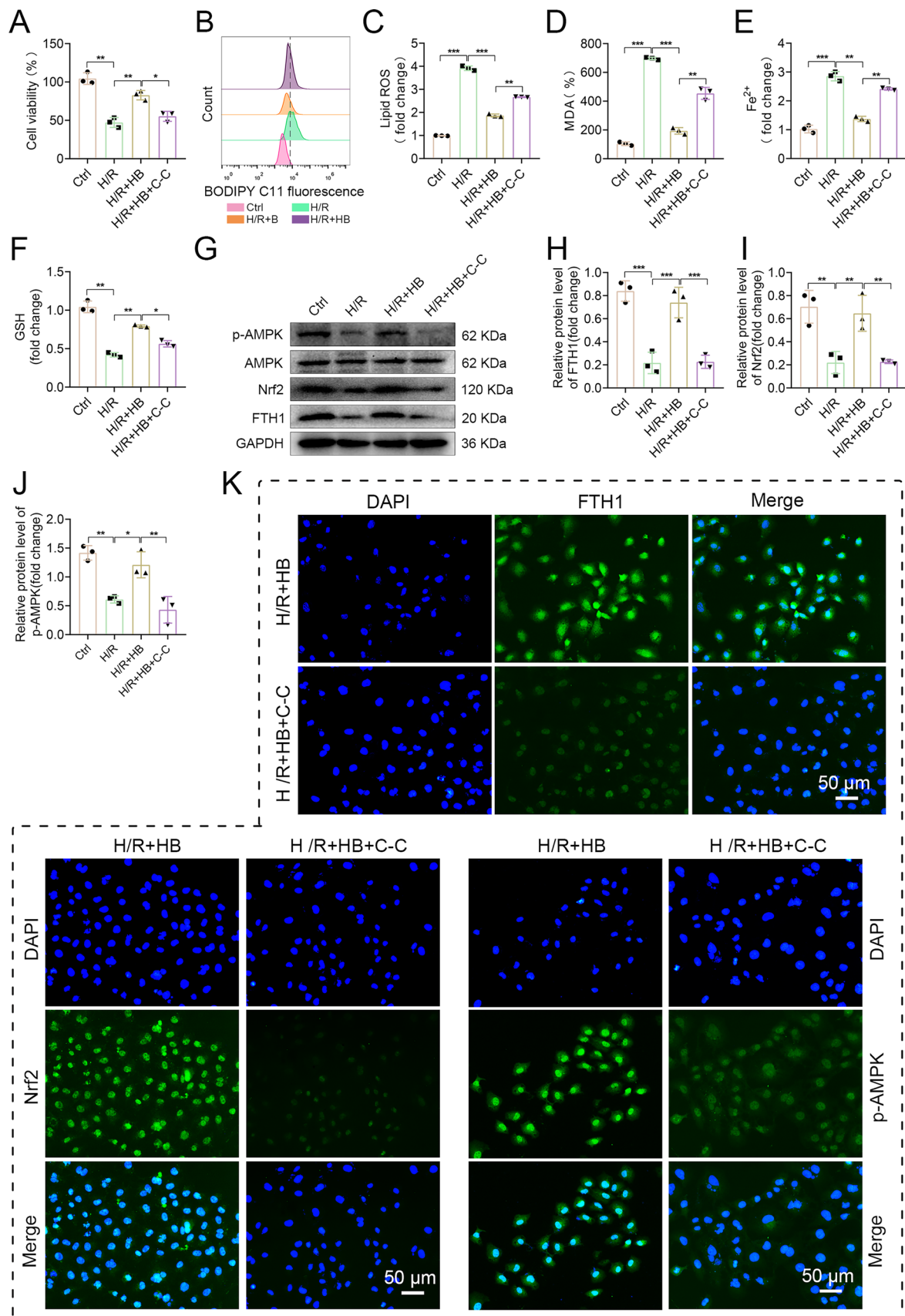


Fig. 5 Effect of AMPK pathway on inhibition of ferroptosis by HO-1/BMMSCs. **A** Measurement of steatotic hepatocyte activity. **B**, **C** Lipid ROS expression in steatotic hepatocytes. **D** Relative MDA expression in steatotic hepatocytes. **E** Relative Fe²⁺ expression in steatotic hepatocytes. **F** Relative GSH expression in steatotic hepatocytes. **G**, **H**, **I**, **J** Relative FTH1 (**H**), Nrf2 (**I**), and p-AMPK (**J**) protein expression. **K** FTH1, Nrf2, and p-AMPK immunofluorescence results (×200). *n* = 3 per group. **p* < 0.05, ***p* < 0.01, ****p* < 0.001

After I/R treatment, the severe steatotic liver had significantly higher CD68 and MPO expression levels than the Sham group, and Fer-1 treatment reversed this trend (Fig. 2C–F). The severe steatotic liver tissue in the IRI group had significantly higher IL-1 β , IL-6, and TNF- α mRNA levels than the Sham and Fer-1 treatment groups (Fig. S6A). The change trends of the liver function markers ALT, AST, TBIL, and LDH were the same as those above (Fig. 2G, H, Fig. S6B). These results indicated that Fer-1 treatment reduced IRI in the rats with severe steatotic liver.

The IRI group had significantly higher MDA, and Fe²⁺, and PTGS2 levels than the Sham group (Fig. 2I–L) and significantly lower GSH levels than the Sham group (Fig. 2K). The IRI group had significantly decreased FTH1 and GPX4 protein expression levels (Fig. 2M–P), where Fer-1 reversed all the above trends (Fig. 2I–P). The above results indicated that ferroptosis was involved in severe steatotic liver IRI in rats.

Both Fer-1 and DFO improved the H/R-induced morphology and activity of the steatotic hepatocytes (Fig. S7A, S7B). The H/R-injured steatotic hepatocytes had significantly altered ROS, lipid ROS, MDA, Fe²⁺, GSH, FTH1, and GPX4 expression levels as compared with the control group, and Fer-1 and DFO significantly improved the H/R-induced changes to the ferroptosis-related indexes (Fig. S7C–L).

HO-1/BMMSCs Inhibited Ferroptosis in Steatotic Liver IRI

In the animal model, the BMMSC and HO-1/BMMSC treatment groups had lower MDA and Fe²⁺ levels than the IRI group (Fig. 3A, B), increased GSH expression levels (Fig. 3C), decreased PTGS2 expression levels (Fig. 3D), and significantly increased FTH1 and GPX4 expression levels (Fig. 3E–H). The above indicators were improved more obviously after HO-1/BMMSC intervention than BMMSC intervention (Fig. 3A–H). These results indicated that the BMMSCs and HO-1/BMMSCs reduced ferroptosis and that the HO-1/BMMSCs exerted more obvious effects.

In the cell model, the BMMSC and HO-1/BMMSC intervention groups had lower ROS, lipid ROS, MDA, and Fe²⁺ levels than the H/R group and significantly increased GSH, FTH1, and GPX4 expression levels. Compared with the

BMMSC group, the HO-1/BMMSC group had more obvious improvement of the above indicators (Fig. S8). These results indicated that both BMMSCs and HO-1/BMMSCs inhibited ferroptosis and that the HO-1/BMMSCs exerted a more significant inhibitory effect.

HO-1/BMMSCs Promoted Nrf2 Expression to Inhibit H/R-induced Ferroptosis in Steatotic Hepatocytes

We successfully knocked down Nrf2 in the steatotic hepatocytes (Fig. S9). In the HO-1/BMMSC group, the H/R-induced steatotic hepatocyte activity was significantly improved, but the activity of steatotic hepatocytes transfected with siRNA against Nrf2 (si-Nrf2) and subjected to the above treatment was not significantly improved (Fig. 4A). Compared with the si-Nrf2 group, HO-1/BMMSCs did not significantly improve lipid ROS, MDA, Fe²⁺, and GSH in the si-Nrf2-transfected steatotic hepatocytes (Fig. 4B–F).

Nrf2 and FTH1 expression in the negative control siRNA (si-NC) group was not significantly different from that in the H/R + HB group, but was significantly higher than that in the H/R group (Fig. 4G–I, K, Fig. S10). Similarly, p-AMPK expression in the si-NC group and the H/R + HB group was not significantly different, but was significantly higher than that in the H/R group (Fig. 4G, J). The fluorescence intensity of Nrf2 nuclei in the H/R + HB and H/R + HB + si-NC groups was significantly enhanced (Fig. 4K, Fig. S10); Nrf2 and FTH1 expression in the si-Nrf2 group was significantly lower than that in the si-NC group (Fig. 4G–I, K), but the p-AMPK expression level was not significantly affected (Fig. 4G, J).

HO-1/BMMSCs promoted Nrf2, FTH1, and p-AMPK expression whereas knocking down Nrf2 significantly reduced FTH1 promotion by HO-1/BMMSCs while also significantly reducing the protective effect of HO-1/BMMSCs on the cells but not significantly affecting p-AMPK expression. It is suggested that HO-1/BMMSCs promoted Nrf2/FTH1 expression, inhibited ferroptosis, and alleviated the damage of H/R-injured steatotic hepatocytes. p-AMPK may be an upstream regulatory molecule of Nrf2. Therefore, we conducted the following study to clarify its relationship with Nrf2/FTH1.

The Role of AMPK in HO-1/BMMSC Alleviation of H/R-Induced Steatotic Hepatocyte Ferroptosis

HO-1/BMMSCs improved the H/R-induced low activity state of the steatotic hepatocytes, while Compound C decreased the improvement ability of HO-1/BMMSCs on cell activity (Fig. 5A). Compared with the H/R + HB group, the H/R + HB + C–C group had significantly increased lipid

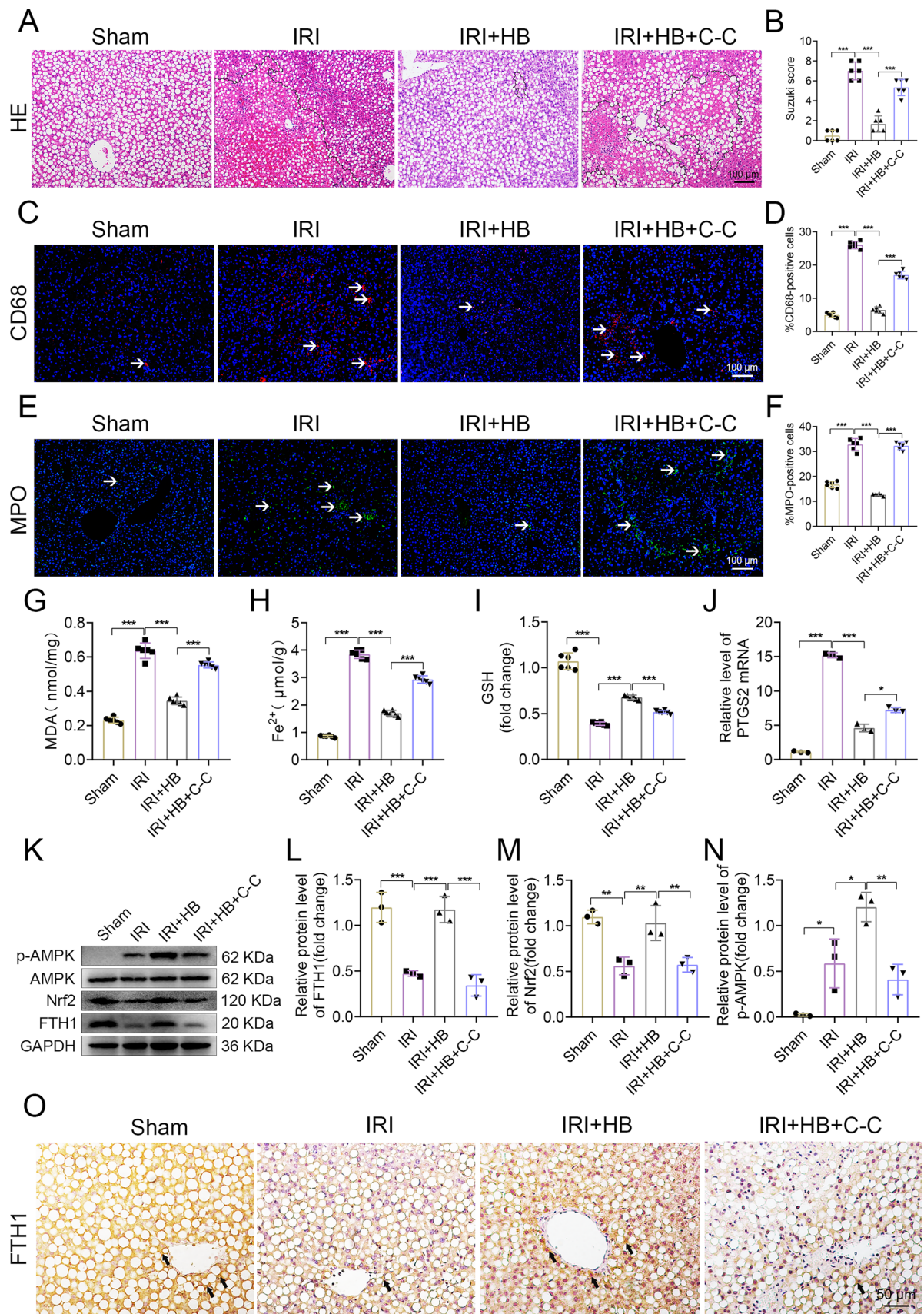


Fig. 6 Effect of blocking AMPK pathway on HO-1/BMMSC inhibition of ferroptosis and protection against severe steatotic liver IRI. **A** Liver histopathology ($\times 100$). **B** Suzuki score of liver tissue. **C, D** CD68 expression (red) in liver tissue ($\times 100$) (white arrows indicate positive-expression cells). **E, F** MPO expression (green) in liver tissue ($\times 100$) (white arrows indicate positive-expression cells). **G** MDA expression in liver tissue. **H** Fe^{2+} expression in liver tissue. **I** GSH expression in liver tissue. **J** PTGS2 expression in liver tissue. **K, L, M, N** FTH1 (**L**), Nrf2 (**M**), and p-AMPK (**N**) protein expression levels in liver tissue. **O** Detection of FTH1 protein in liver tissue ($\times 200$). Black arrows indicate positive-expression cells. $n=6$ per group. * $p < 0.05$, ** $p < 0.01$, *** $p < 0.001$

ROS, MDA, and Fe^{2+} levels (Fig. 5B–E) and significantly decreased GSH level (Fig. 5F).

Compared with the H/R group, the FTH1, Nrf2, and p-AMPK expression levels in the H/R + HB group were significantly higher (Fig. 5G–K, Fig. S11). Compared with the H/R + HB group, the FTH1, Nrf2, and p-AMPK expression levels in the Compound C-treated cells were significantly reduced (Fig. 5G–K). The above results indicated that blocking the AMPK pathway significantly reduced the protective effects of HO-1/BMMSCs on H/R-induced ferroptosis and cell damage in the steatotic hepatocytes. HO-1/BMMSCs attenuated the H/R-induced ferroptosis-dependent AMPK pathway in steatotic hepatocytes through Nrf2–FTH1.

AMPK–Nrf2–FTH1 Is Involved in HO-1/BMMSC Inhibition of Ferroptosis and Alleviation of IRI in Rats

Compared with the IRI + HB group, the necrosis area and degree of liver tissue congestion in the IRI + HB + C–C group were significantly increased (Fig. 6A). Furthermore, the Suzuki score was significantly increased (Fig. 6B) and the CD68, MPO, IL-1 β , IL-6, and TNF- α expression levels were significantly increased (Fig. 6C–F, Fig. S12A), as were ALT, AST, TBIL, and LDH levels (Fig. S12B). The results suggested that blocking the AMPK pathway weakened the protective effect of HO-1/BMMSCs on rat steatotic liver IRI.

The IRI + HB + C–C group had significantly higher MDA and Fe^{2+} levels than the IRI + HB group (Fig. 6G, H), significantly decreased GSH level (Fig. 6I), and increased PTGS2 expression (Fig. 6J). The results indicated that blocking the AMPK pathway weakened the inhibitory effect of HO-1/BMMSCs on ferroptosis. Compared with the IRI + HB group, the IRI + HB + C–C group had significantly decreased FTH1, Nrf2, and p-AMPK expression levels (Fig. 6K–O). This was consistent with the *in vitro* results, indicating that blocking the AMPK pathway reduced Nrf2 and FTH1 expression, aggravated ferroptosis, and reduced the protective effect of HO-1/BMMSCs on steatotic liver IRI in rats.

Discussion

The large gap between the demand for liver transplantation and the availability of donor livers remains a great challenge for the liver transplantation community [23]. Due to the increasing incidence of non-alcoholic fatty liver disease (NAFLD) worldwide and the shortage of donor livers in many countries, the use of donor grafts with hepatic steatosis is now more common [24]. As the donor liver fat content increases, so does the risk of graft dysfunction after liver transplantation [25]. Severe steatotic liver is more sensitive to IRI, and the survival rate of the donor liver in the recipient post-transplantation is significantly reduced [5, 6]. Therefore, it is particularly important to explore means of reducing the IRI of donor livers with severe steatosis to alleviate the donor liver shortage and prolong the recipients' long-term survival.

MSCs are an effective therapeutic tool that have also been applied in related research of liver diseases [26]. Our results demonstrated that BMMSCs and HO-1/BMMSCs alleviated severe steatotic liver IRI in rats and that the HO-1/BMMSCs exerted a stronger repairing effect. This might have been due to the antioxidant activity of HO-1 alone, which has the strong ability to protect cells during ischemia [27]. We modified MSCs with HO-1 to enhance the MSC colonization ability and biological activity in damaged organs [27, 28]. We co-cultured the BMMSCs and HO-1/BMMSCs each with severe steatotic hepatocytes and determined that the BMMSCs and HO-1/BMMSCs exerted a protective effect against H/R-induced severe steatotic hepatocyte injury, where the protective effect of HO-1/BMMSCs was more significant. The protection mechanism was related to the extracellular vesicles secreted by MSCs [29–31]. In this study, the repair and paracrine effects of the HO-1/BMMSCs were significantly enhanced as compared with that of pure MSCs [32].

In recent years, ferroptosis has been observed in IRI of various organs [9–11]. Primarily driven by iron-dependent phospholipid peroxidation, ferroptosis is regulated by multiple cellular metabolisms, including redox homeostasis, iron metabolism, mitochondrial activity, fat, amino acid, and glucose metabolism, and multiple metabolic pathways associated with various diseases [33]. We evaluated the degree of ferroptosis in severe steatotic liver with IRI, where the IRI group had a severe degree of ferroptosis and Fer-1 inhibited ferroptosis and alleviated IRI. We also evaluated the degree of ferroptosis in severe steatotic hepatocytes under H/R conditions and determined that the H/R group had a severe degree of ferroptosis and that both Fer-1 and DFO inhibited ferroptosis and improved the H/R-induced cell damage. The results demonstrated that ferroptosis was involved in severe steatotic liver IRI. The ferroptosis evaluation results of the

BMMSC and HO-1/BMMSC groups revealed that both BMMSCs and HO-1/BMMSCs inhibited ferroptosis, where the HO-1/BMMSCs exerted a stronger inhibitory effect. These findings suggested that HO-1/BMMSCs reduced IRI in severe steatotic liver by inhibiting ferroptosis, which was consistent with the findings of Wu et al. [29]. Therefore, how do HO-1/BMMSCs regulate ferroptosis in this condition and play a protective role?

Ferritin is the main iron-binding protein in non-hematopoietic tissues, which can limit the catalytic role of iron in oxygen free radical generation and participate in antioxidant reactions [34]. Furthermore, FTH1 reduces IRI in the liver [35], lysosomes dissolve ferritin, thereby increasing the level of free iron [36], while Fe^{2+} overload enhances oxidative stress through the Fenton-like reaction, producing a large number of ROS and consequently promoting ferroptosis [37]. FTH1 is important in resisting ferroptosis by maintaining cellular iron homeostasis [38]. In this study, the IRI group had increased Fe^{2+} and decreased FTH1 levels, but HO-1/BMMSC treatment reversed the change trend of the two indexes, and the *in vitro* results were consistent with the *in vivo* results. It is suggested that HO-1/BMMSCs may reduce lipid peroxidation levels by adjusting the FTH1 content, thereby slightly inhibiting ferroptosis.

Nrf2 is a major regulator of antioxidant responses and is important in maintaining intracellular homeostasis [39, 40]. Regulating Nrf2 can improve liver enzyme disorders, hepatocyte damage, and the inflammatory reactions associated with I/R [40–43]. Nrf2 induces FTH1 expression [44–46]. In this study, the HO-1/BMMSCs promoted FTH1 expression and improved the degree of liver injury and ferroptosis. We used the steatotic hepatocyte model of Nrf2 knockdown to clarify whether HO-1/BMMSCs can play an anti-ferroptosis role through Nrf2–FTH1. We determined that the HO-1/BMMSC-pretreated steatotic hepatocytes had significantly increased Nrf2 and FTH1 expression compared with the H/R group. si-Nrf2 treatment significantly decreased Nrf2 and FTH1 expression and the cell antioxidant capacity while significantly increasing lipid ROS accumulation, which indicated that HO-1/BMMSCs activated Nrf2 in IRI with severe steatotic liver.

AMPK is a highly conserved major metabolic regulator, and its activation is related to the treatment of many metabolic diseases, including NAFLD [47, 48]. IRI research revealed that activated AMPK reduced oxidative stress and the inflammatory reaction [49, 50]. Inactivating AMPK greatly weakened the protective effect of ferroptosis-related renal IRI [51]. Many studies reported that regulating the AMPK–Nrf2 pathway can regulate ferroptosis to reduce the damage of the target organs [52–54], but are few reports

in IRI of severe steatotic liver. In this study, AMPK was activated after HO-1/BMMSC treatment and promoted Nrf2 and FTH1 expression. Similarly, HO-1/BMMSC intervention in the H/R model of severe steatotic hepatocytes *in vitro* activated AMPK and increased Nrf2 and FTH1 expression. We used Compound C *in vitro* and *in vivo* to examine whether Nrf2 activation by the HO-1/BMMSCs was AMPK-dependent. We determined that inhibiting the AMPK pathway significantly decreased Nrf2 and FTH1 expression and significantly reduced the ability of HO-1/BMMSCs to inhibit ferroptosis. However, p-AMPK expression was not significantly affected in the Nrf2 knockout group, indicating that AMPK is the upstream regulator of Nrf2 and that HO-1/BMMSC activation of Nrf2–FTH1 to inhibit ferroptosis and protect against steatotic liver IRI was AMPK-dependent.

Conclusion

We demonstrated that HO-1/BMMSCs exerted a protective effect on IRI in severe steatotic liver and that ferroptosis was involved in IRI in severe steatotic liver. The HO-1/BMMSCs inhibited ferroptosis protection in IRI by activating the AMPK–Nrf2–FTH1 pathway. The findings suggested a new method for studying the clinical application of donor liver with severe steatosis and provided a research direction for expanding the donor liver pool.

Supplementary Information The online version contains supplementary material available at <https://doi.org/10.1007/s10620-023-08102-0>.

Author's contribution X-RT and H-LS conceived and designed experiments. X-RT, Y-XW, M-SY, W-PZ, H-WZ and X-RZ conducted the experiments and obtained the results. X-RT and H-LS sorted and analyzed the results; X-RT and H-LS wrote the draft. X-RT and H-LS extensively revised, formatted, and submitted versions of the manuscript. All authors participated in data discussions. All authors read and approved the final manuscript.

Funding The work was supported by the National Natural Science Foundation of China (Nos. 82070639, 81670574, 81441022, and 81270528).

Declarations

Conflict of interest The authors declare that there are no conflicts of interest regarding the publication of this paper.

Ethical approval All animals were treated in strict accordance with the Guidelines for the Care and Use of Experimental Animals and the protocol was approved by the Animal Ethics Committee of Nankai University (License No.: 2021-SYDWLL-000331).

Consent for publication Not applicable.

Open Access This article is licensed under a Creative Commons Attribution-NonCommercial 4.0 International License, which permits any

non-commercial use, sharing, adaptation, distribution and reproduction in any medium or format, as long as you give appropriate credit to the original author(s) and the source, provide a link to the Creative Commons licence, and indicate if changes were made. The images or other third party material in this article are included in the article's Creative Commons licence, unless indicated otherwise in a credit line to the material. If material is not included in the article's Creative Commons licence and your intended use is not permitted by statutory regulation or exceeds the permitted use, you will need to obtain permission directly from the copyright holder. To view a copy of this licence, visit <http://creativecommons.org/licenses/by-nc/4.0/>.

References

- Jadlowiec CC, Taner T. Liver transplantation: Current status and challenges. *World J Gastroenterol*. 2016;22:4438–4445.
- Duell PB, Welty FK, Miller M et al. Nonalcoholic Fatty Liver Disease and Cardiovascular Risk: A Scientific Statement From the American Heart Association. *Arterioscler Thromb Vasc Biol*. 2022;42:e168–e185.
- Cheng YF, Yu CY, Ou HY, et al. Section 1. Image evaluation of fatty liver in living donor liver transplantation. *Transplantation*. 2014;97 Suppl 8:S3–6.
- Ito T, Naini BV, Markovic D et al. Ischemia-reperfusion injury and its relationship with early allograft dysfunction in liver transplant patients. *Am J Transplant*. 2021;21:614–625.
- Tashiro H, Kuroda S, Mikuriya Y, Ohdan H. Ischemia–reperfusion injury in patients with fatty liver and the clinical impact of steatotic liver on hepatic surgery. *Surg Today*. 2014;44:1611–1625.
- Schleicher J, Dahmen U. Computational Modeling of Oxidative Stress in Fatty Livers Elucidates the Underlying Mechanism of the Increased Susceptibility to Ischemia/Reperfusion Injury. *Comput Struct Biotechnol J*. 2018;16:511–522.
- Wu B, Song HL, Yang Y et al. Improvement of Liver Transplantation Outcome by Heme Oxygenase-1-Transduced Bone Marrow Mesenchymal Stem Cells in Rats. *Stem Cells Int*. 2016;2016:9235073.
- Podestà MA, Remuzzi G, Casiraghi F. Mesenchymal Stromal Cell Therapy in Solid Organ Transplantation. *Front Immunol*. 2021;11:618243.
- Yu P, Zhang J, Ding Y et al. Dexmedetomidine post-conditioning alleviates myocardial ischemia-reperfusion injury in rats by ferroptosis inhibition via SLC7A11/GPX4 axis activation. *Hum Cell*. 2022;35:836–848.
- Qi D, Chen P, Bao H et al. Dimethyl fumarate protects against hepatic ischemia-reperfusion injury by alleviating ferroptosis via the NRF2/SLC7A11/HO-1 axis. *Cell Cycle*. 2023;22:818–828.
- Ma D, Li C, Jiang P, Jiang Y, Wang J, Zhang D. Inhibition of Ferroptosis Attenuates Acute Kidney Injury in Rats with Severe Acute Pancreatitis. *Dig Dis Sci*. 2021;66:483–492.
- Hirschhorn T, Stockwell BR. The development of the concept of ferroptosis. *Free Radic Biol Med*. 2019;133:130–143.
- Jia M, Qin D, Zhao C et al. Redox homeostasis maintained by GPX4 facilitates STING activation. *Nat Immunol*. 2020;21:727–735.
- Bersuker K, Hendricks JM, Li Z et al. The CoQ oxidoreductase FSP1 acts parallel to GPX4 to inhibit ferroptosis. *Nature*. 2019;575:688–692.
- Yan HF, Tuo QZ, Yin QZ, Lei P. The pathological role of ferroptosis in ischemia/reperfusion-related injury. *Zool Res*. 2020;41:220–230.
- Li X, Wu L, Tian X et al. miR-29a-3p in Exosomes from Heme Oxygenase-1 Modified Bone Marrow Mesenchymal Stem Cells Alleviates Steatotic Liver Ischemia-Reperfusion Injury in Rats by Suppressing Ferroptosis via Iron Responsive Element Binding Protein 2. *Oxid Med Cell Longev*. 2022;2022:6520789.
- Li S, Zhu Z, Xue M et al. The protective effects of fibroblast growth factor 10 against hepatic ischemia-reperfusion injury in mice. *Redox Biol*. 2021;40:101859.
- Matzinger M, Fischhuber K, Pölöske D, Mechtler K, Heiss EH. AMPK leads to phosphorylation of the transcription factor Nrf2, tuning transactivation of selected target genes. *Redox Biol*. 2020;29:101393.
- Zeng B, Lin G, Ren X, Zhang Y, Chen H. Over-expression of HO-1 on mesenchymal stem cells promotes angiogenesis and improves myocardial function in infarcted myocardium. *J Biomed Sci*. 2010;17:80.
- Eggenhofer E, Rovira J, Sabet-Baktach M et al. Unconventional ROR γ t+ T cells drive hepatic ischemia reperfusion injury. *J Immunol*. 2013;191:480–487.
- Suzuki S, Toledo-Pereyra LH, Rodriguez FJ, Cejalvo D. Neutrophil infiltration as an important factor in liver ischemia and reperfusion injury. Modulating effects of FK506 and cyclosporine. *Transplantation*. 1993;55:1265–72.
- Yang L, Cao H, Sun D et al. Normothermic Machine Perfusion Combined with Bone Marrow Mesenchymal Stem Cells Improves the Oxidative Stress Response and Mitochondrial Function in Rat Donation After Circulatory Death Livers. *Stem Cells Dev*. 2020;29:835–852.
- Bodzin AS, Baker TB. Liver Transplantation Today: Where We Are Now and Where We Are Going. *Liver Transpl*. 2018;24:1470–1475.
- Vinaixa C, Selzner N, Berenguer M. Fat and liver transplantation: clinical implications. *Transpl Int*. 2018;31:828–837.
- McCormack L, Clavien PA. Understanding the meaning of fat in the liver. *Liver Transpl*. 2005;11:137–139.
- Kang HT, Jun DW, Jang K et al. Effect of Stem Cell Treatment on Acute Liver Failure Model Using Scaffold. *Dig Dis Sci*. 2019;64:781–791.
- Yan X, Cheng X, He X, Zheng W, Yuan X, Chen H. HO-1 Over-expressed Mesenchymal Stem Cells Ameliorate Sepsis-Associated Acute Kidney Injury by Activating JAK/stat3 Pathway. *Cell Mol Bioeng*. 2018;11:509–518.
- Cao H, Wu L, Tian X et al. HO-1/BMMSc perfusion using a normothermic machine perfusion system reduces the acute rejection of DCD liver transplantation by regulating NKT cell co-inhibitory receptors in rats. *Stem Cell Res Ther*. 2021;12:587.
- Wu L, Tian X, Zuo H et al. miR-124-3p delivered by exosomes from heme oxygenase-1 modified bone marrow mesenchymal stem cells inhibits ferroptosis to attenuate ischemia-reperfusion injury in steatotic grafts. *J Nanobiotechnology*. 2022;20:196.
- Wechsler ME, Rao VV, Borelli AN, Anseth KS. Engineering the MSC Secretome: A Hydrogel Focused Approach. *Adv Healthc Mater*. 2021;10:e2001948.
- Wu P, Zhang B, Shi H, Qian H, Xu W. MSC-exosome: A novel cell-free therapy for cutaneous regeneration. *Cytherapy*. 2018;20:291–301.
- Chen X, Wu S, Tang L et al. Mesenchymal stem cells overexpressing heme oxygenase-1 ameliorate lipopolysaccharide-induced acute lung injury in rats. *J Cell Physiol*. 2019;234:7301–7319.
- Jiang X, Stockwell BR, Conrad M. Ferroptosis: mechanisms, biology and role in disease. *Nat Rev Mol Cell Biol*. 2021;22:266–282.
- Tsuji Y, Ayaki H, Whitman SP, Morrow CS, Torti SV, Torti FM. Coordinate transcriptional and translational regulation of ferritin in response to oxidative stress. *Mol Cell Biol*. 2000;20:5818–5827.
- Berberat PO, Katori M, Kaczmarek E et al. Heavy chain ferritin acts as an antiapoptotic gene that protects livers from ischemia reperfusion injury. *FASEB J*. 2003;17:1724–1726.

36. Sun R, Liu M, Xu K et al. Ferroptosis is involved in the benzene-induced hematotoxicity in mice via iron metabolism, oxidative stress and NRF2 signaling pathway. *Chem Biol Interact.* 2022;362:110004.
37. Li LX, Guo FF, Liu H, Zeng T. Iron overload in alcoholic liver disease: underlying mechanisms, detrimental effects, and potential therapeutic targets. *Cell Mol Life Sci.* 2022;79:201.
38. Tian Y, Lu J, Hao X et al. FTH1 Inhibits Ferroptosis Through Ferritinophagy in the 6-OHDA Model of Parkinson's Disease. *Neurotherapeutics.* 2020;17:1796–1812.
39. Rao J, Qiu J, Ni M et al. Macrophage nuclear factor erythroid 2-related factor 2 deficiency promotes innate immune activation by tissue inhibitor of metalloproteinase 3-mediated RhoA/ROCK pathway in the ischemic liver. *Hepatology.* 2022;75:1429–1445.
40. Xu D, Xu M, Jeong S et al. The Role of Nrf2 in Liver Disease: Novel Molecular Mechanisms and Therapeutic Approaches. *Front Pharmacol.* 2019;9:1428.
41. Ahmed O, Xu M, Zhou F et al. NRF2 assessment in discarded liver allografts: A role in allograft function and salvage. *Am J Transplant.* 2022;22:58–70.
42. Ge M, Yao W, Yuan D et al. Brg1-mediated Nrf2/HO-1 pathway activation alleviates hepatic ischemia-reperfusion injury. *Cell Death Dis.* 2017;8:e2841.
43. Xu D, Chen L, Chen X et al. The triterpenoid CDDO-imidazolide ameliorates mouse liver ischemia-reperfusion injury through activating the Nrf2/HO-1 pathway enhanced autophagy. *Cell Death Dis.* 2017;8:e2983.
44. Ramos S, Carlos AR, Sundaram B et al. Renal control of disease tolerance to malaria. *Proc Natl Acad Sci U S A.* 2019;116:5681–5686.
45. Seiwert N, Wecklein S, Demuth P et al. Heme oxygenase 1 protects human colonocytes against ROS formation, oxidative DNA damage and cytotoxicity induced by heme iron, but not inorganic iron. *Cell Death Dis.* 2020;11:787.
46. Zhao Y, Zhang R, Wang Z et al. Melatonin Prevents against Ethanol-Induced Liver Injury by Mitigating Ferroptosis via Targeting Brain and Muscle ARNT-like 1 in Mice Liver and HepG2 Cells. *J Agric Food Chem.* 2022;70:12953–12967.
47. Garcia D, Hellberg K, Chaix A et al. Genetic Liver-Specific AMPK Activation Protects against Diet-Induced Obesity and NAFLD. *Cell Rep.* 2019;26:192–208.e6.
48. Oakhill JS, Scott JW, Kemp BE. Structure and function of AMP-activated protein kinase. *Acta Physiol (Oxf).* 2009;196:3–14.
49. Awad H, Nolette N, Hinton M, Dakshinamurti S. AMPK and FoxO1 regulate catalase expression in hypoxic pulmonary arterial smooth muscle. *Pediatr Pulmonol.* 2014;49:885–897.
50. Song P, Zou MH. Regulation of NAD(P)H oxidases by AMPK in cardiovascular systems. *Free Radic Biol Med.* 2012;52:1607–1619.
51. Lee H, Zandkarimi F, Zhang Y et al. Energy-stress-mediated AMPK activation inhibits ferroptosis. *Nat Cell Biol.* 2020;22:225–234.
52. Wang X, Chen X, Zhou W et al. Ferroptosis is essential for diabetic cardiomyopathy and is prevented by sulforaphane via AMPK/NRF2 pathways. *Acta Pharm Sin B.* 2022;12:708–722.
53. Wang S, Yi X, Wu Z et al. CAMKK2 Defines Ferroptosis Sensitivity of Melanoma Cells by Regulating AMPK-NRF2 Pathway. *J Invest Dermatol.* 2022;142:189–200.e8.
54. Lu H, Xiao H, Dai M, Xue Y, Zhao R. Britanin relieves ferroptosis-mediated myocardial ischaemia/reperfusion damage by upregulating GPX4 through activation of AMPK/GSK3 β /Nrf2 signalling. *Pharm Biol.* 2022;60:38–45.

Publisher's Note Springer Nature remains neutral with regard to jurisdictional claims in published maps and institutional affiliations.